PROPAGATION FACTOR AND PATH LOSS SIMULATION RESULTS FOR TWO ROUGH SURFACE REFLECTION COEFFICIENTS APPLIED TO THE MICROWAVE DUCTING PROPAGATION OVER THE SEA

I. Sirkova

Microwave Physics & Technologies Lab
Institute of Electronics, Bulgarian Academy of Sciences
72 Tzarigradsko Chaussee, Sofia 1784, Bulgaria

Abstract—The performance assessment of maritime microwave communications and radar systems requires accounting simultaneously for the non-homogeneous propagation medium over the sea and the rough sea surface scattering. The tropospheric ducting, specific for over water propagation, is one of the most difficult to treat propagation mechanisms. The proposed work combines a recently published in the literature phase correction, responsible for the shadowing effects, to the Ament rough surface reflection coefficient and the Parabolic Equation method (as implemented in the Advanced Propagation Model) to simulate the microwave propagation over the sea under evaporation duct conditions. Propagation factor and path loss results calculated for phase-corrected Ament, non-phase-corrected Ament and the other widely used, Miller-Brown, rough surface reflection coefficient are compared and discussed. The main effects from the accounting of the shadowing result in the shift of the interference minima and maxima of the propagation factor, changes in the path loss pattern and destruction of the trapping property of the duct.

1. INTRODUCTION

In coastal and maritime regions the microwave propagation is affected by the high variability with space and time of the meteorological parameters. This variability leads to respective changes in the tropospheric refractive index n [1, 2]. The vertical change of the refractivity N ($N = (n - 1)10^6$) is of predominant importance and

Table 1. Refractive condition types.

Refraction types	dN/dz N-Units/km	dM/dz M-Units/km
a) subrefraction	$dN/dz > 0$	$dM/dz > 157$
b) normal	$0 \geq dN/dz > -79$	$157 \geq dM/dz > 78$
standard troposphere	$dN/dz = -39.2$	$dM/dz = 118$
c) superrefraction	$-79 \geq dN/dz > -157$	$78 \geq dM/dz > 0$
d) ducting	$dN/dz \leq -157$	$dM/dz \leq 0$

the gradient dN/dz values determine four refractive condition types reported in Table 1 where the relations are given also in terms of modified refractivity M [1–3]. The modified refractivity is defined as $M = N + (z/a_e)10^6$ with z the height above the surface and a_e — the earth's radius. The introduction of M is made for two reasons: a) the appearance of negative M gradient indicates immediately the formation of the most severe case among the four refractive condition types — the ducting; b) the introduction of M allows the use of the flattened-Earth concept [2] when one is interested in low heights above the Earth surface.

The ducting is present for small percent of time but it seriously influences the radar [3, 4] and communications systems [5–8] working in the microwave range: the rays' bending under ducting differs from that for standard troposphere and provokes erroneous precipitation detection by ground-based meteorological radars, the electromagnetic energy trapping within the ducts leads to trans-horizon signal propagation, reflections from upper refractive layers cause mulipath fading, etc. Depending on the physical mechanism of their formation, the tropospheric ducts are subdivided in different types — here we are interested in evaporation ducts for which the negative gradient of M is due to evaporation from large bodies of water [9]. Ducts due to evaporation are a common occurrence above the sea at lower latitudes and even in moderate latitudes they are not an occasional event [3, 10]. The ducting over water and in flat coastal areas is considered to be the major short-term interference mechanism [11] in these regions. The increase of frequency sharing between different radar and communications systems makes the accurate prediction of signals likely to cause interference even for a short time an important task [12]; still more this is true for regions affected by ducting.

The correct assessment of the coverage of the maritime microwave systems requires simultaneous accounting for the non-homogeneous

propagation medium over the sea and the rough sea surface scattering. There is no rigorous solution to this problem suitable for practical usage. The parabolic equation (PE) approximate technique, proven to be computationally fast and accurate in handling wave propagation in complex environments, is often used with the effects of roughness incorporated through an approximate rough surface reflection coefficient [13–17]. In the propagation over the ocean studies, the surface roughness effects are accounted for by defining an "effective" reflection coefficient, R_{eff}, representing the Fresnel reflection coefficient from flat surface multiplied by a Roughness Reduction Factor (RRF) [14]. Two RRFs have been widely used: the Ament coefficient [18] and Miller-Brown one [19]. The comparisons of the propagation prediction results obtained with these two rough surface reflection coefficients to the propagation measurements do not allow concluding which of them is more accurate neither there is in the open literature a definitive explanation of some discrepancies between the propagation modeling and the observed experimental results — see the discussions in [20–22]. Both correcting coefficients affect only the magnitude of the complex Fresnel reflection coefficient by multiplying it with a real number. Recently, theoretical investigations have been carried out in order to improve the accuracy in accounting for the effects of ocean roughness on radio wave propagation by introducing a phase correction, responsible for the shadowing, to the Ament coefficient [23]. At grazing incidence angles under which the electromagnetic energy trapping occurs in the ducts, the non-accounting for the shadowing may lead to a wrong prediction of the field strength and overestimation of the coverage range.

The proposed work combines the phase-corrected Ament RRF obtained in [23] and the PE method as implemented in the Advanced Propagation Model (APM) [14, 24] to compute the propagation factor (PF) for microwave propagation over the ocean under evaporation duct conditions. A comparison is made between the PFs calculated for phase-corrected Ament, non-phase-corrected Ament and Miller-Brown rough surface reflection coefficients. Path loss (PL) results are given as well. The introduction of the shadowing in the propagation model leads to the following main effects: shift of the interference minima and maxima of the propagation factor, changes in the path loss pattern, reduction of the long-range ducted propagation.

2. THEORETICAL BACKGROUNDS

In this section, a brief description is given of the shadowing due to sea surface roughness and the PE method as used later in the paper.

The introduction of the shadowing follows strictly [23]. In [23], a Probability Density Function (PDF) has been derived for the *illuminated* points only of a one-dimensional rough surface with Gaussian statistics of heights and slopes and for forward propagation. This newly derived illumination height PDF has been used to obtain the RRF R_{rf} (1) which accounts for the shadowing [23]:

$$R_{rf} = \exp\left(-iQ\tilde{m}_\xi - \frac{Q^2\tilde{\sigma}_\xi^2}{2}\right) \tag{1}$$

where:

$$Q = 2k\sin(\varphi), \tag{2}$$

$$\tilde{\sigma}_\xi = \sqrt{2}\sigma_\xi\tilde{\sigma}_z, \, \tilde{m}_\xi = \sqrt{2}\sigma_\xi\tilde{m}_z, \tag{3}$$

$$\tilde{m}_z(\upsilon) = \frac{1+2\Lambda}{\sqrt{\pi}}\int_{-\infty}^{\infty} z\exp\left(-z^2\right)\left(1 - \frac{\mathrm{erfc}(z)}{2}\right)^{2\Lambda} dz, \tag{4}$$

$$\tilde{\sigma}_z^2(\upsilon) = \frac{1+2\Lambda}{\sqrt{\pi}}\int_{-\infty}^{\infty} (z-\tilde{m}_z)^2\exp\left(-z^2\right)\left(1 - \frac{\mathrm{erfc}(z)}{2}\right)^{2\Lambda} dz, \tag{5}$$

$$\upsilon = \frac{\tan(\varphi)}{\sqrt{2}\sigma_\gamma} \, , \, \Lambda(\upsilon) = \frac{\exp\left(-\upsilon^2\right) - \upsilon\sqrt{\pi}\mathrm{erfc}(\upsilon)}{2\upsilon\sqrt{\pi}}. \tag{6}$$

In the above formulae k is the wave number in free space; φ is the plane wave grazing incidence angle to the rough surface; ξ and γ are the surface height and slope; σ_ξ and σ_γ are the standard deviations of ξ and γ, respectively; $z = \xi/(2^{1/2}\sigma_\xi)$ stands for the normalized height; $\tilde{m}_\xi$, $\tilde{\sigma}_\xi$ and $\tilde{m}_z$, $\tilde{\sigma}_z$ are the mean value and standard deviation of the illuminated surface heights and the illuminated normalized heights, respectively. The RRF (1) is obtained using the same statistics as the one assumed for the derivation of the original Ament RRF, R_A, given by (7) [18]:

$$R_A = \exp\left[-2k^2\sigma_\xi^2\sin^2(\varphi)\right]. \tag{7}$$

Expression (8) below gives the Miller-Brown RRF, R_{M-B}, [19]. In (7) and (8) the parameters k, σ_ξ and φ have the same meanings as in (1); I_0 in (8) is the modified Bessel function of the first kind of order zero.

$$R_{M-B} = \exp\left[-2k^2\sigma_\xi^2\sin^2(\varphi)\right] \, \mathrm{I}_0\left[2k^2\sigma_\xi^2\sin^2(\varphi)\right]. \tag{8}$$

Note that the RRF (1) not only introduces a phase to the Ament's correction coefficient R_A (7) but also corrects its amplitude by the introduction of $\tilde{\sigma}_\xi$ instead of σ_ξ (this is not just an intuitive inclusion

of a phase change to account for the path difference between rough and smooth surface in the case of plane wave incidence as it is done in [20]). Note also that the R_{M-B} (8) is derived using PDF obtained for sea surface formed by random variable whose amplitude has Gaussian distribution with zero mean and whose phase is uniformly distributed in the interval $[-\pi/2, \pi/2]$ — this statistics differs from the statistics for which $\tilde{m}_\xi$ and $\tilde{\sigma}_\xi$ in (1) are obtained, i.e., their automatic application to Miller-Brown coefficient will not be correct.

The "effective" reflection coefficient R_{eff} is defined as [14]:

$$R_{eff} = R_{rfac}R_F \qquad (9)$$

where R_F is the complex Fresnel reflection coefficient from smooth flat surface and the RRF R_{rfac} is given by (1), (7) or (8).

To use the above formula one needs values for σ_ξ and σ_γ. They are given by relations (10), see [23] for details on their derivation, where u_{10} is the wind speed at 10 meters above the sea surface:

$$\sigma_\xi \approx 6.28 \times 10^{-3} u_{10}^{2.02}, \quad \sigma_\gamma \approx 5.62 \times 10^{-2} u_{10}^{0.5}. \qquad (10)$$

Formulae (1)–(10) combined with the Advanced Propagation Model (APM) routines [24], which are based on a hybrid ray optics/PE method, are used to compute the PF and PL for microwave propagation over rough sea in the presence of evaporation duct. The parameters of the problem (grazing angles, low altitudes) require mainly the use of the PE-based part of the APM for which the electromagnetic field calculations are based on the two-dimensional (2D) narrow-angle forward-scatter scalar PE [14] given by (11):

$$\frac{\partial U(x,z)}{\partial x} = \frac{i}{2k} \frac{\partial^2 U(x,z)}{\partial z^2} + \frac{ik}{2} \left(m^2(x,z) - 1 \right) U(x,z). \qquad (11)$$

The PE method, and especially its 2D form (11), is well documented in the literature [13–17, 25, 26], so that here a very brief explanation is given. As paraxial approximation, the PE assumes the problem has some "preferred" propagation direction, say, the x-axis in a Cartesian coordinate system. In (11), independence of all quantities from y coordinate is assumed, k is the free-space wave number, $m = M10^{-6}+1$ is the modified refractive index, $U(x,z)$ is the reduced or slow-varying along the preferred propagation direction function obtained by factoring out the rapid fluctuations (the term $\exp(ikx)$) of a transverse field component Ψ (E or H depending on the polarization), x and z stay for range and altitude. Equation (11) is obtained from the scalar wave equation after applying the far-field approximation (i.e., assuming $kx \gg 1$) and the paraxial approximation (which means that $|\partial^2 U/\partial x^2| \ll k|\partial U/\partial x|$). In addition, $m^2(x,z)$ must be slowly varying function in the direction of "preferred" propagation. The

PE (11) has the advantage to be easily solved numerically through marching algorithms provided the field is known on an initial plane and adequate boundary conditions on the boundaries in the domain of interest are given. The primary drawback of the PE is that it neglects the backscattering which may be important when treating propagation over rough surfaces [25]. The tropospheric ducting problem involves electromagnetic field variations over scales much larger than the wavelength and grazing incident angles. Under these conditions the forward-propagated field plays dominant role [25]. This, with the gently undulation of the sea surface and smooth variation of the tropospheric refractive index with x assures the applicability of the paraxial approximation and (11) to the studied problem. Equation (11) is very accurate at angles within $\pm 15°$ of the preferred direction of propagation [14].

The APM [24] is based on a split-step Fourier-transform (SSF) solution of the PE [13, 14]. The SSF allows larger step sizes and shorter computational time in comparison to Finite Difference [14] and Finite Element [17] based numerical solutions of (11), [14]. The last makes SSF adequate to solve long-range tropospheric radiowave propagation problems. In APM the PE is combined with the impedance boundary condition at the earth surface for the transverse field components [13]:

$$\left.\frac{\partial \Psi}{\partial z}\right|_{z=0} + \alpha_{h,v}\left.\Psi\right|_{z=0} = 0, \tag{12}$$

$$\alpha_{h,v} = ik\sin\left(\varphi\right)\frac{1 - R_{eff}}{1 + R_{eff}}, \tag{13}$$

where $\alpha_{h,v}$ is the surface impedance term with subscripts h, v referring to horizontal and vertical polarization, φ is the local grazing angle, Ψ is the respective field component depending on the polarization. Relation (13) provides direct relation of $\alpha_{h,v}$ to the surface reflection coefficient thus allowing the introduction of the roughness effects through the "effective" reflection coefficient, R_{eff}, which substitutes the smooth-surface Fresnel reflection coefficient in (13). The SSF solution of (11) subject to the impedance boundary condition (12), (13), firstly derived in [13] and further improved in [27], is used in APM. A wide-angle propagator is also included that allows treating propagation problems requiring larger propagation angles with respect to the horizon; see [16] and the discussion in [15] about the introduction of the wide-angle propagator. The local grazing angles φ are determined by a combination of spectral estimation and geometric optics methods [15, 24]. The surface impedance characteristics are calculated as a function of frequency using permittivity and conductivity graphs given in [28]. In order

to insure the radiation condition and prevent spurious reflections from the upper computational window boundary, an attenuation function (Tukey "window") is used to "filter" the field strength in the highest $1/4$ of the calculation domain [16, 24]. The initial field $U(0, z)$ required to start the calculation procedure is obtained using the relation between the far-field antenna pattern $F(p)$ and the aperture field distribution $A(z)$ which form a Fourier transform pair [14, 16]. Applying the boundary condition for perfectly conducting surface and image theory, $U(0,z)$ is expressed through $A(z - z_a)$ and $A^*(z + z_a)$ where z_a is the antenna height. By Fourier-transforming $U(0, z)$ one obtains the reduced function $U(0, p)$ in angle (or p) space expressed via $F(p)$ (which is normally a known function):

$$\breve{U}(0, p) = F(p) \exp(-ipz_a) - F^*(-p) \exp(ipz_a),$$
$$\breve{U}(0, p) = F(p) \exp(-ipz_a) + F^*(-p) \exp(ipz_a),$$

(14)

where $p = k \sin(\theta)$ is the transform variable, θ is the angle from the horizontal, the first of Equation (14) refers to horizontal polarization, the second refers to vertical polarization. The antenna height is accounted for using the Fourier shift theorem; similarly, the antenna elevation angle θ_s may be included in (14) by replacing $F(p)$ by $F(p - p_s)$ where $p_s = k \sin(\theta_s)$. Finally, $U(0, z)$ is obtained applying inverse Fourier transform to (14).

The PE and APM have been extensively validated through simulations and measurements for different complicated environments, including the case of tropospheric ducting propagation, see [6, 8, 16, 26].

In this study, the initial field is provided by an omni directional antenna (i.e., $F(p) = 1$ for all angles θ) and the PF (in decibels) is defined as the square of the ratio of the electric field amplitude E at a given point under specific conditions to the electric field amplitude E_0 received at the same point under free-space conditions where E participates with its polarization component which coincides with the polarization of E_0 [2]. Equation (15) gives the expression of the PF in terms of the reduced PE field $U(x, z)$ as well as the relation between the PF and the quantity usually considered in radiowave propagation problems, the path loss, PL (PL in dB), [14]:

$$PF = 20 \log |U(x, z)| + 10 \log(r) + 10 \log(\lambda), \; PL = 20 \log \left(\frac{4\pi r}{\lambda} \right) - PF,$$

(15)

where λ is the free-space wavelength, r is the distance between the corresponding points and the first term in the right-hand side of the expression for the PL denotes the free-space loss.

3. RESULTS AND DISCUSSION

The implementation of the formulae accounting for the shadowing into the APM was tested through comparisons with simulation results reported in [23] for the case of standard troposphere, see Table 1. Figure 1(a) shows an example of PF, computed with phase-corrected Ament RRF and APM, plotted versus height for fixed range. The parameters used for Figure 1(a) coincide with those for Figure 5 from [23]: frequency $F = 5\,\text{GHz}$, distance from the transmitter $r = 5\,\text{km}$, transmitter height $z_a = 5\,\text{m}$, wind speed $u_{10} = 7\,\text{m/s}$ (corresponding to $\sigma_\xi = 0.33$, $\sigma_\gamma = 0.15$), dielectric characteristics of the sea surface: relative permittivity $= 80.0$ and conductivity $= 4.0\,\text{S/m}$, horizontal polarization. On Figure 1(b), the curve from Figure 1(a) is superimposed on Figure 5 from [23]. A good agreement is seen between the red curve, computed with APM, and the continuous black line from [23] (the dashed curves on Figure 1(b) belong to the results of [23] and do not refer to the work presented here).

For ducting propagation conditions, the evaporation duct is modelled by log-linear height profile of the modified refractivity M, (16), [29]:

$$M(z) = M_0 + 0.13 \left[z - z_d \ln \left(\frac{z + z_0}{z_0} \right) \right], \qquad (16)$$

where z_0 is the aerodynamic roughness parameter taken to be $1.5 \times 10^{-4}\,\text{m}$ [14], $M_0 = M(z = 0)$, z_d — the duct thickness. In [29], Equation (16) has been obtained assuming thermally neutral troposphere, thus (16) does not account for the stability effects on
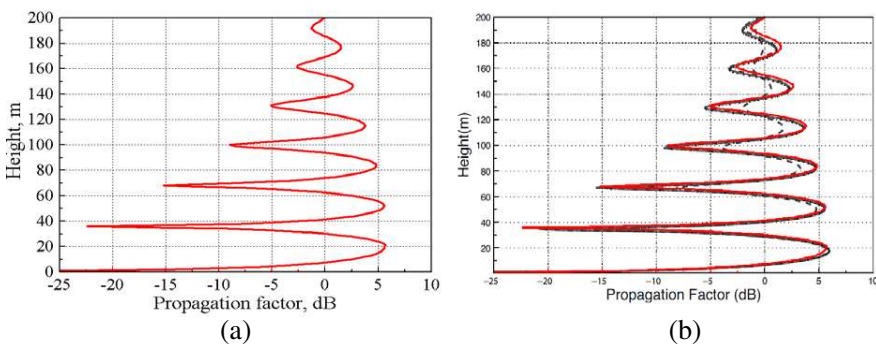

Figure 1. (a) Propagation factor computed through APM with phase-corrected Ament RRF and standard troposphere conditions; (b) the curve from (a) superimposed on Figure 5 from [23].

the $M(z)$ profile [14]. Nevertheless, propagation calculations and measurements have shown this neutral profile is a good practical approximation to the average behavior of the $M(z)$ [30] and (16) has been widely used as input to propagation modeling under evaporation duct conditions [7, 8, 14, 17, 30]. Further discussion on the profile (16) may be found in [9].

All following examples are for vertically polarized waves. The PF versus height is plotted at fixed ranges. The PL is plotted versus range and height. As demonstrated in [23], the shadowing effect introduced through RRF (1) has small influence on the PF if the ratio $\beta = \sigma_\xi/\lambda$ is close or lower than unity. The results reported here refer to values of $\sigma_\xi = 0.33$ and $\sigma_\xi = 0.66$ (corresponding to wind speed $u_{10} = 7\,\text{m/s}$ and $u_{10} = 10\,\text{m/s}$, respectively) and frequencies $F = 5\,\text{GHz}$ and $F = 10\,\text{GHz}$. The respective values of β are sufficiently higher than unity to make the effect of shadowing manifested: $\beta = 5.5$ and 11 for $\sigma_\xi = 0.33$; $\beta = 11$ and 22 for $\sigma_\xi = 0.66$.

Figure 2 presents comparisons between PFs obtained with RRFs given by Equations (1), (7) and (8) for standard troposphere, (a), and evaporation duct conditions, (b). The parameters used are: frequency $F = 5\,\text{GHz}$, antenna height $z_a = 5\,\text{m}$, range from the source $r = 5\,\text{km}$, $u_{10} = 7\,\text{m/s}$; $M(z)$ profile for Figure 2(b) is obtained for $z_d = 14\,\text{m}$. Clearly seen is the shift of the interference minima and maxima of the PF due to the phase correction in the RRF (1) as well the changes in the maxima and minima magnitudes (the places of the maxima and
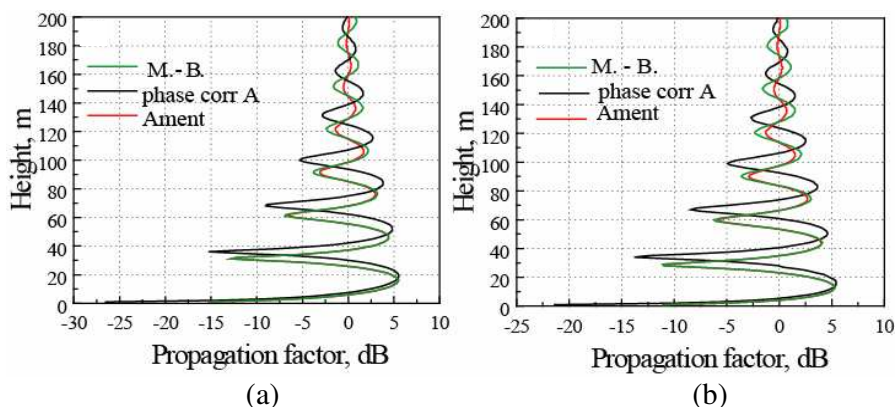

Figure 2. Comparison between PFs obtained for phase-corrected Ament, Miller-Brown and original Ament RRFs, $F = 5\,\text{GHz}$, $z_a = 5\,\text{m}$, $r = 5\,\text{km}$, $u_{10} = 7\,\text{m/s}$; (a) standard troposphere conditions; (b) evaporation duct conditions, $z_d = 14\,\text{m}$.

minima of the PF for the case of flat surface reflection coefficient (not shown in the picture) coincide with those of the PFs for Miller-Brown and original Ament reflection coefficients). At this short distance, the duct has (almost) not changed the pattern of the PF, computed with different RRFs, in comparison to that under standard troposphere. The increase of the distance and/or the frequency makes the influence of the ducting more evident. Figure 3 provides the same comparisons as Figure 2 but for $F = 10\,\text{GHz}$, $r = 10\,\text{km}$.
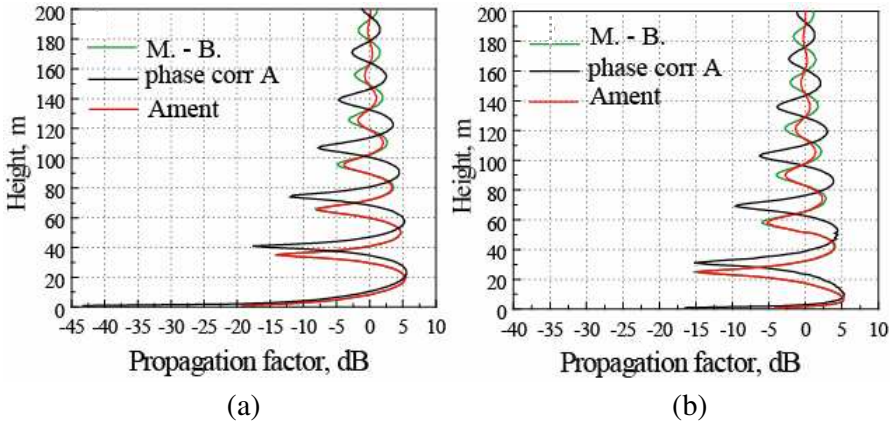

Figure 3. Same as Figure 2 except $F = 10\,\text{GHz}$, $r = 10\,\text{km}$.

The duct "presses" the PF pattern minima and maxima to the underlying surface and changes their magnitudes. The decrease with height of the oscillations of the Miller-Brown-based PF happens slowly than that of the original Ament-based PF. This, with the setting aside of the displacement which increases with height, makes the pattern of the Miller-Brown-based PF from Figures 2 and 3 to appear formally closer to those obtained from (1) than the pattern of the PF based on the original Ament RRF.

The effect of different RRFs on microwave PL for the case of ducting propagation is shown in Figures 4 and 5 where $F = 10\,\text{GHz}$, $z_d = 14\,\text{m}$, $z_a = 5\,\text{m}$ for the first Figure and $F = 5\,\text{GHz}$, $z_d = 25\,\text{m}$, $z_a = 5\,\text{m}$ for the second one. In Figures 4(a) and 5(a) the PL is calculated for smooth sea. For both Figures 4 and 5, (b) and (c) show PL for Miller-Brown RRF with $u_{10} = 7\,\text{m/s}$ and $u_{10} = 10\,\text{m/s}$ (corresponds to $\sigma_\xi = 0.66$, $\sigma_\gamma = 0.18$), respectively; PL in (d) and (e) is obtained under the same values of u_{10} as for (b) and (c) but for original Ament RRF; (f) and (g) refer to PL based on phase-corrected Ament RRF with the same values of u_{10} as for (b) and (c).

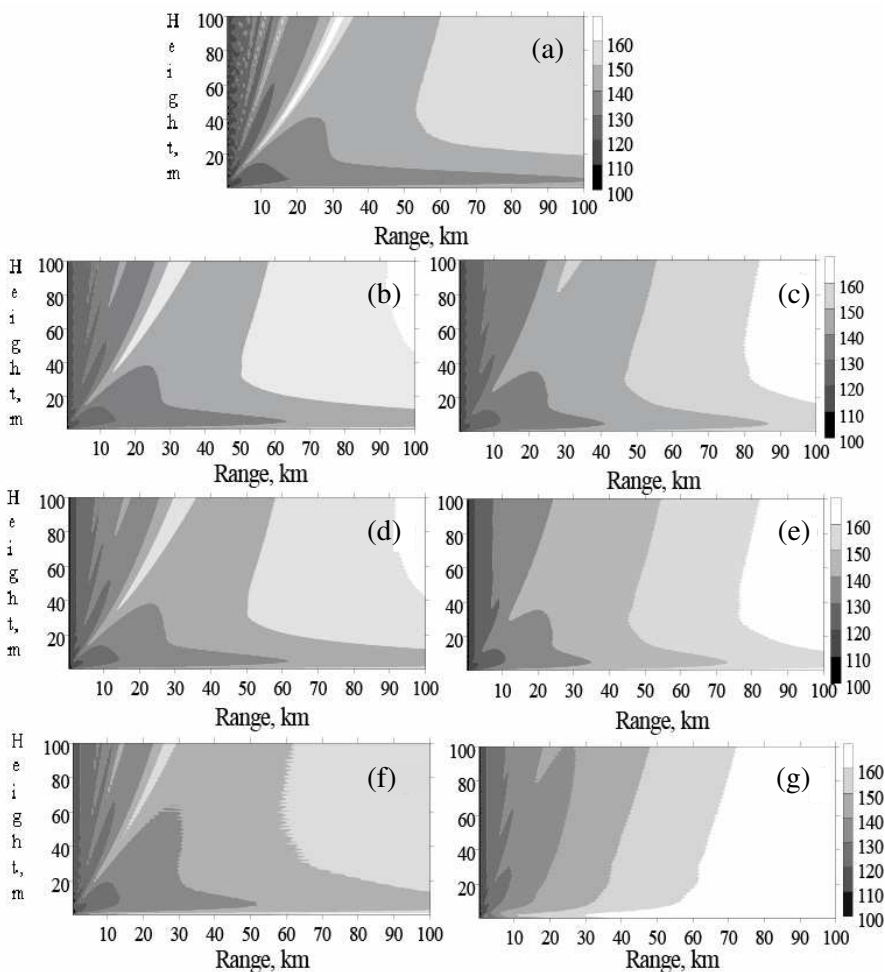In general, the surface roughness changes the PL pattern and

Figure 4. Path loss for evaporation duct conditions, $F = 10\,\text{GHz}$, $z_d = 14\,\text{m}$, $z_a = 5\,\text{m}$: (a) smooth sea; (b), (c) Miller-Brown RRF with $u_{10} = 7\,\text{m/s}$ and $u_{10} = 10\,\text{m/s}$, respectively; (d), (e) original Ament RRF with $u_{10} = 7\,\text{m/s}$ and $u_{10} = 10\,\text{m/s}$, respectively; (f), (g) phase-corrected Ament RRF with $u_{10} = 7\,\text{m/s}$ and $u_{10} = 10\,\text{m/s}$, respectively. The right-hand side color bar provides the PL levels in dB.

destroys the trapping property of the duct structure. Under the specific propagation parameters used here (especially the low heights), the Miller-Brown and original Ament RRFs give very similar PL patterns, the first one being closer to the smooth surface case. It appears that
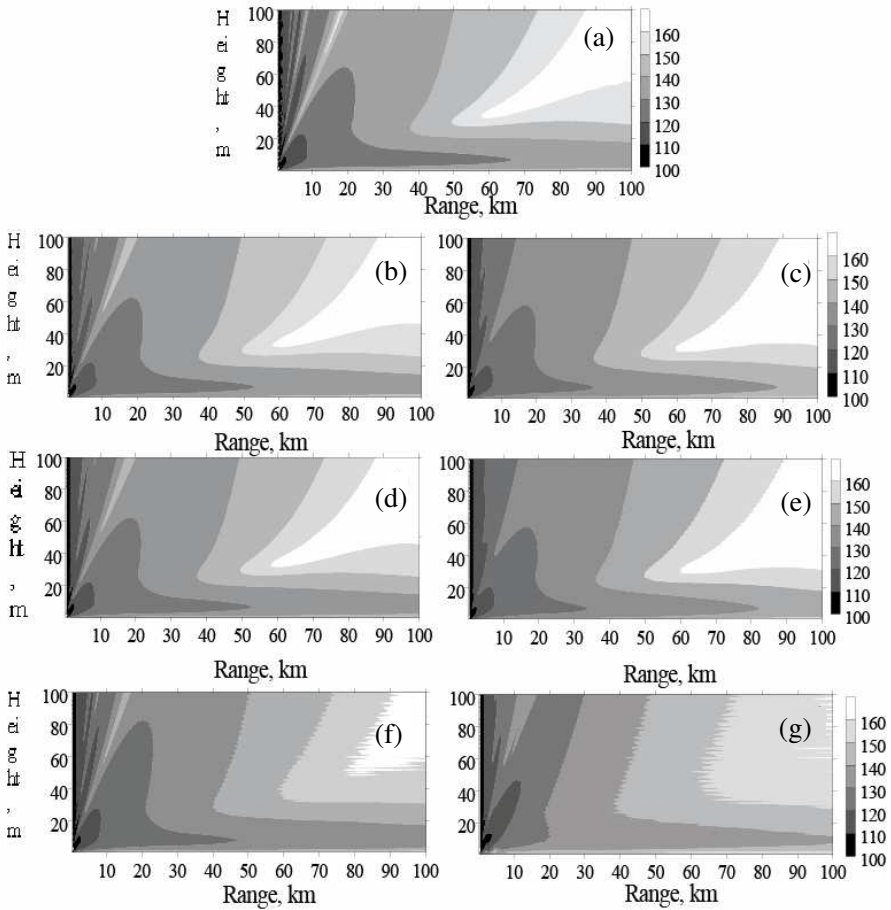
Figure 5. Path loss for evaporation duct conditions, $F = 5\,\text{GHz}$, $z_d = 25\,\text{m}$, $z_a = 5\,\text{m}$: (a) smooth sea; (b), (c) Miller-Brown RRF with $u_{10} = 7\,\text{m/s}$ and $u_{10} = 10\,\text{m/s}$, respectively; (d), (e) original Ament RRF with $u_{10} = 7\,\text{m/s}$ and $u_{10} = 10\,\text{m/s}$, respectively; (f), (g) phase-corrected Ament RRF with $u_{10} = 7\,\text{m/s}$ and $u_{10} = 10\,\text{m/s}$, respectively. The right-hand side color bar provides the PL levels in dB.

the phase-corrected Ament RRF is the most "destructive" especially as far the long-range ducted propagation is concerned: the PL pattern in Figure 4(g) for $u_{10} = 10\,\text{m/s}$ resembles more the standard troposphere PL pattern than that of ducted propagation over smooth sea given in Figure 4(a). Figure 4(g) indicates that the expected strong increase of the coverage which is characteristic of ducted propagation will not be

predicted if the shadowing is included in the propagation model.

The strong duct ($z_d = 25\,\mathrm{m}$) under which Figure 5 is obtained still preserves the energy trapping but for phase-corrected Ament RRF the PL pattern is "scattered" even for the lower $u_{10} = 7\,\mathrm{m/s}$, see (f) and (g) from Figure 5. This result is expected because the RRF (1) reduces in greatest degree (in comparison to (7) and (8)) the specular scattering thus reducing the coherence between the direct and reflected field.

For over sea propagation, the PL predictions based on the phase-corrected Ament RRF should be considered more reliable than those based on (7) or (8) [23] but it is to note that (1) neglects the diffraction on the rough surface. The wind direction which also influences the propagation over rough sea [31] as well as other mechanisms responsible for the sea roughness are not accounted for in this study.

4. CONCLUSION

This work presents the effects of the shadowing, as introduced in [23], on the microwave propagation over rough sea surface under evaporation duct conditions. The inclusion of the shadowing is expected to improve the propagation modeling and increase the coincidence between predicted and measured field in this complicated environment. For long-range ducted propagation, due to the repeated reflections and grazing angles, the effect of shadowing is expected to increase. The higher frequencies are better guided by the duct but the criterion $\beta = \sigma_\xi/\lambda$ implies that the increase of the frequency increases the importance of the shadowing and thus the long-range propagation of higher frequencies is impeded. Subject of future investigation may be the relation between the pairs {duct thickness-duct strength} and {σ_ξ, λ}. The accounting for the wind direction and the influence of other mechanisms leading to sea roughness besides the wind may be combined with the shadowing effect.

The RRF (1) is only one possible way to introduce the shadowing which was made under the supposition of Gaussian statistics of the surface. As mentioned in [21], the statistics may differ from Gaussianity. A possible future investigation is to search if the shadowing or the deviation from the Gaussianity has more influence on the propagation factor. A further development of the presented study may be the implementation of tri-dimensional PE which will allow the inclusion of the diffuse scattering.

The examples reported here and the above considerations demonstrate the need of additional investigations, both theoretical and experimental, on the rough sea surface scattering. The acquired knowledge will help transmission power, frequency and angle

adjustments in order to improve microwave systems performance under the complicated propagation conditions in coastal and maritime areas.

REFERENCES

1. ITU-R P.453-9, "The radio refractive index: Its formula and refractivity data," 27, ITU, 2003.
2. Kerr, D. E., *Propagation of Short Radio Waves*, Peninsula Publishing, Los Altos, 1988.
3. Lopez, P. H., "A 5-yr 40-km-resolution global climatology of superrefraction for ground-based weather radars," *J. Appl. Meteor. Climatol.*, Vol. 48, 89–110, Jan. 2009.
4. Anderson, K. D., "Radar detection of low-altitude targets in a maritime environment," *IEEE Trans. Antennas Propag.*, Vol. 43, No. 6, 609–613, Jun. 1995.
5. Woods, G. S., A. J. Kerans, and D. L. Maskell, "Simulated angle-of-arrival measurements for an over ocean microwave radio link," *Proc. URSI Commission F Triennium Open Symposium*, 200–207, Cairns, Australia, Jun. 2004.
6. Barrios, A. E., K. Anderson, and G. Lindem, "Low altitude propagation effects — A validation study of the advanced propagation model (APM) for mobile radio applications," *IEEE Trans. Antennas Propag.*, Vol. 54, No. 10, 2869–2877, Oct. 2006.
7. Sirkova, I. and M. Mikhalev, "Parabolic-equation-based study of ducting effects on microwave propagation," *J. Microw. Opt. Technol. Letters*, Vol. 42, No. 5, 390–394, Sep. 2004.
8. Gunashekar, S. D., E. M. Warrington, D. R. Siddle, and P. Valtr, "Signal strength variations at 2 GHz for three sea paths in the British channel islands: Detailed discussion and propagation modeling," *Radio Sci.*, Vol. 42, RS4020, Aug. 2007, doi: 10.1029/2006RS003617.
9. Babin, S. M., G. S. Young, and J. A. Carton, "A new model for the oceanic evaporation duct," *J. Appl. Meteor.*, Vol. 36, No. 3, 193–204, Mar. 1997.
10. Von Engeln, A. and J. Teixeira, "A ducting climatology derived

from ECMWF global analysis fields," *J. Geophys. Res.*, Vol. 109, D18104, Sep. 2004, doi: 10.1029/2003JD004380.

11. ITU-R P.452-11, "Prediction procedure for the evaluation of microwave interference between stations on the surface of the earth at frequencies above about 0.7 GHz," 38, ITU, 2003.

12. Milas, V. F. and P. H. Constantinou, "Interference environment between high altitude platform networks (HAPN), geostationary (GEO) satellite and wireless terrestrial systems," *Wireless Personal Communications*, Vol. 32, No. 3–4, 257–274, Feb. 2005.

13. Kuttler, J. R. and G. D. Dockery, "Theoretical description of the parabolic approximation/fourier split-step method of representing electromagnetic propagation in the troposphere," *Radio Sci.*, Vol. 26, No. 2, 381–393, Mar.–Apr. 1991.

14. Levy, M., *Parabolic Equation Methods for Electromagnetic Wave Propagation*, The Institution of Electrical Engineers, London, UK, 2000.

15. Donohue, D. J. and J. R. Kuttler, "Propagation modeling over terrain using the parabolic wave equation," *IEEE Trans. Antennas Propag.*, Vol. 48, No. 2, 260–277, Feb. 2000.

16. Barrios, A., "A terrain parabolic equation model for propagation in the troposphere," *IEEE Trans. Antennas Propag.*, Vol. 42, No. 1, 90–98, Jan. 1994.

17. Sirkova, I. and M. Mikhalev, "Parabolic wave equation method applied to the tropospheric ducting propagation problem — A survey," *Electromagnetics*, Vol. 26, No. 2, 155–173, Feb. 2006.

18. Ament, W. S., "Toward a theory of reflection by a rough surface," *Proc. IRE*, Vol. 41, No. 1, 142–146, Jan. 1953.

19. Miller, A. R., R. M. Brown, and E. Vegh, "New derivation for the rough surface reflection coefficient and for the distribution of sea-wave elevations," *IEE Proc. Microwaves, Optics and Antennas*, Vol. 131, Part H, No. 2, 114–116, Apr. 1984.

20. Freund, D. E., N. E. Woods, H.-C. H. Ku, and R. S. Awadallah, "Forward radar propagation over a rough sea surface: A numerical assessment of the Miller-Brown approximation using a horizontally polarized 3-GHz line source," *IEEE Trans. Antennas Propag.*, Vol. 54, No. 4, 1292–1304, Apr. 2006.

21. Hristov, T. S., K. D. Anderson, and C. A. Friehe, "Scattering properties of the ocean surface: The Miller-Brown-Vegh model revisited," *IEEE Trans. Antennas Propag.*, Vol. 56, No. 4, 1103–1109, Apr. 2008.

22. Freund, D. E., N. E. Woods, H.-C. Ku, and R. S. Awadallah,

"The effects of shadowing on modelling forward radar propagation over a rough sea surface," *Waves in Random and Complex Media*, Vol. 18, No. 3, 387–408, Aug. 2008.

23. Fabbro, V., C. Bourlier, and P. F. Combes, "Forward propagation modelling above Gaussian rough surfaces by the parabolic wave equation: Introduction of the shadowing effect," *Progress In Electromagnetics Research*, Vol. 58, 243–269, 2006.

24. Barrios, A. E. and W. L. Patterson, "Advanced propagation model (APM) Computer software configuration item (CSCI) documents," *Space and Naval Warfare Systems Command Tech.*, Doc. 3145, 479, San Diego, CA, 2002.

25. Awadallah, R. S., "Rough surface scattering and propagation over rough terrain in ducting environments," Doctoral Dissertation, 189, Virginia Polytechnic Institute and State University, Blacksburg, Virginia, 1998.

26. Apaydin, G. and L. Sevgi, "The split-step-fourier and finite-element based parabolic-equation propagation prediction tools: Canonical tests, systematic comparisons, and calibration," *IEEE Antennas Propag. Magazine*, Vol. 52, No. 3, 66–79, Jun. 2010.

27. Dockery, G. D. and J. R. Kuttler, "An improved impedance-boundary algorithm for Fourier split-step solutions of the parabolic wave equation," *IEEE Trans. Antennas Propag.*, Vol. 44, No. 12, 1592–1599, Dec. 1996.

28. Recommendations and Reports of the CCIR, "Propagation in non-ionized media," *CCIR XVth Plenary Assembly*, Vol. 5, ITU, Geneva, Dubrovnik, 1986.

29. Rotheram, S., "Radiowave propagation in the evaporation duct," *Marconi Review*, Vol. 37, No. 192, 18–40, 1974.

30. Paulus, R. A. and K. D. Anderson, "Application of an evaporation duct climatology in the littoral," *Proc. Battlespace Atmospheric and Cloud Impacts on Military Operations, BACIMO*, 1–9, Fort Collins, Colorado, Apr. 2000.

31. Smith, Jr., J. R., S. J. Russell, B. E. Brown, P. M. Haldeman, Jr., D. D. Hayden, D. G. Morgan, R. D. Pierce, J. W. Shan, W. T. Stephens, and M. S. Mirotzni, "Electromagnetic forward-scattering measurements over a known, controlled sea surface at low grazing," *IEEE Trans. Geosci. Remote Sensing*, Vol. 42, No. 6, 1197–1207, Jun. 2004.